

Turbulence in Coronal Mass Ejections

A. A. Ruzmaikin, J. Feynman, and E. J. Smith

Jet Propulsion Laboratory, California Institute of Technology, Pasadena

Short title: TURBULENCE IN CMES

Abstract. The magnetic fields measured by the ISEE 3 spacecraft are used to study MHD turbulence within coronal mass ejections (CMEs). The spectral indices of the turbulence inside CMEs are compared with spectral indices found in solar wind undisturbed by CMEs. Irrespective of the CME velocities, the spectra within CMEs are found to differ from those determined for the fast solar wind from coronal holes. Instead, the CME spectra more closely resemble those found in the slow solar wind. Since both CMEs and the plasma sheet are associated with closed magnetic structures in the solar corona, it appears that the turbulence in the solar wind arising from closed coronal regions is fundamentally different from the turbulence in wind from coronal holes.

The helical properties of the CME magnetic fields are also studied. Preliminary results indicate that randomly distributed smaller scale helical disturbances accompany the largescale helical structure of the CMEs.

Introduction

Three distinct types of the solar wind have been identified: fast quasi-stationary solar wind from coronal holes, slow solar wind accelerated in the vicinity of coronal streamers, and intermittent solar wind produced by coronal mass ejections (CMEs). These solar winds differ in many respects [Feldman, 1996; Gosling, 1996; Zwickl et al., 1983]. MHD studies of the fast and slow solar wind have indicated interesting differences in the turbulence in these two regimes. The turbulence is characterized by the spectral index of the variations from the mean field. In both the fast and slow wind the turbulence contains a high frequency regime in which the spectral index is in the neighborhood of $-5/3$ (for reviews see Roberts and Goldstein, [1990]; Tu and Marsch, [1995]). This turbulence is said to be Kolmogorov-like. (In the study reported here we do not discuss changes to the observed spectral index due to the intermittency [Ruzmaikin et al., 1995].) This Kolmogorov-like regime is believed to be due to turbulence developing in situ as the solar wind propagates from the Sun to the point of observation. Small scale turbulence develops first and the turbulent cascade proceeds to longer wavelengths with time or distance from the Sun [Tu and Marsch, 1995]. For the fast solar wind from coronal holes the spectrum flattens to a value closer to -1 at lower frequencies. This low frequency turbulence is believed to arise from the Sun itself. The flattening is not as evident for the slow solar wind within the heliospheric current sheet [Tu and Marsch, 1995]. In addition to the energy spectra studies much of attention has been focused on helicity of magnetic fluctuations in the solar wind, since helicity is a conserved quantity [Matthaeus and Goldstein, 1982; Goldstein et al., 1995].

Turbulence within CMEs has attracted less attention. Here we study that turbulence and compare it to turbulence in wind from coronal holes and coronal streamers. We also present results from a study of magnetic helicity in a limited number of CMEs and samples of the fast and slow wind.

The data

We use 1 minute averaged magnetic field data obtained by the ISEE 3 satellite in 1978-1982 when it was in the vicinity of the Earth. CMEs propagating in the solar wind carry solar plasma that can be distinguished from plasma in other types of solar wind by a number of signatures including counterstreaming fluxes of superthermal electrons [Gosling, 1990], magnetic clouds [Burlaga *et al.*, 1981], enhancements in the abundance of helium nuclei relative to protons [Hirshberg *et al.*, 1972] and others. These distinguishes typically are not all present at the same time and a given CME may exhibit only a selected few of the many markers that have been studied [Zwickl *et al.*, 1983]. CMEs are not distinguished by solar wind velocity except in rare cases of very high speed events [Hundhausen., 1996].

To study turbulence we use twelve bidirectional electron streaming events (BES) identified by Gosling *et al.*, [1987], see also [Neugebauer and Alexander, 1991] and six magnetic clouds (MC) identified by Lepping *et al.*, [1990]. We do not use the helium enhancement events because the enhancement identification was unreliable (Gosling, personal communication) and there are so few long duration events of this type. We use five samples of coronal hole wind and ten samples of slow solar wind not associated with holes and identified by Neugebauer and Alexander, [1991]. These ten samples are divided into low velocity wind clearly associated with the current heliospheric sheet (plasma sheet flows, PS) and low velocity wind not containing a current sheet (interstreams, IS). The intervals are listed in Tables 1 and 2. Examples of the magnetic fields in the solar wind coming from a coronal hole and from a CME identified as a magnetic cloud are shown in Figure 1 and Figure 2 respectively.

Magnetic Energy Spectra in CMEs

The magnetic and velocity fields in the solar wind are composed of mean values and superposed fluctuations of a complicated nature. The fluctuations are essentially random; that is they have continuous power spectra which can be characterized by their slopes, i.e. spectral indices. A simple way to obtain the spectral index is to use the second-order structure function constructed directly in the observational time domain:

$$S(\tau) = \frac{1}{3} \sum_{i=1}^3 \langle |B_i(t + \tau) - B_i(t)|^2 \rangle \quad (1)$$

where the sum is taken over all three components of the magnetic field and averaging $\langle \rangle$ is taken over the interval of data used. In the coordinate system used throughout this paper the axis x is along the radial direction and positive outward from the Sun, y is in the ecliptic plane and positive in the direction of planetary motion and z is perpendicular to x and y and positive north. The structure function defined by Eq. (1) is equivalent to the spectrum determined by the invariant trace of the field fluctuations. However, instead of the frequency, a time scale variable τ is used. For power-law spectra the structure function has also a power-law form $S(\tau) \propto \tau^{1+\alpha}$, where α is the standard spectral exponent [Monin and Yaglom, 1975]. An advantage of the structure function is that it is unaffected by data gaps. The presence of data gaps just decreases the statistical number of points at a given scale τ .

An example of a structure function of a high speed wind from a coronal hole is shown in the upper panel of Figure 3. The two spectral regions are clearly discerned: a high-frequency (small τ 's) Kolmogorov-like turbulence and a low-frequency $1/f$ noise-like spectrum. The break point is at about 1/2 hour. The form the spectrum agrees well with those reported in the studies referenced above. In the work that follows we will compute the spectral indices for frequency ranges above and below 1/2 hour separately. Spectral indices for the five samples of solar wind from coronal holes are given in Table 1. The uncertainties of the indices shown in the last two columns are

formal uncertainties calculated from the line fitting program. The actual uncertainties are larger because the accuracy of the values of a spectral index depends on the size of a data. In addition, each data string is a sample of the random process (turbulence) and therefore gives only a spectral index for a realization of that process. We estimate that the indices shown have an actual uncertainty of about 0.1.

An example of a structure function for a slow solar wind associated with an interstream are shown in the second panel of Figure 3. The results for other cases are presented in Table 1. The high frequency spectrum is much the same as for the coronal hole but the low frequency spectrum exhibits a much steeper slope. The average change in slope from the high-frequency to low frequency range for the entire sample of non-CME wind corresponds to a flattening of about 0.4.

An example of a structure function for a CME with bidirectional electron streaming is shown in the third panel of Figure 3. Again, the high frequency spectral index is the same as in the upper two panels. However in this case there is no break in the spectrum. The low frequency spectrum has the same spectral index. On average the low frequency spectral indices of all the CME events in Table 2 corresponds to a steepening of 0.04. This is consistent with no change at all. A glance at Table 2 will show that three of the spectra steepen to values exceeding 2. If these are considered anomalous and omitted from the calculation of the mean change, it is found that the mean change would be a flattening of 0.05. This flattening is 1/10 that for the non-CME sample and is again consistent with no change in spectral index within CMEs.

In Figure 4 we compare the spectral indices for coronal hole wind with that for CMEs. In the high-frequency range (lower panel) there is only a small difference between the indices for the two types of solar wind. However, in the low-frequency range (the upper panel) the spectral indices within CMEs are larger than those in the coronal hole wind. The difference is statistically significant. To illustrate this a line has been drawn at an arbitrary value of 1.4. Five of the five coronal hole samples lie below

that line whereas 16 of the 17 CME spectral indices fall above it. The probability that this happen by chance is very small. Thus the turbulence in CMEs differs significantly from that in quasi-steady wind from a coronal hole.

Also notice the three cases in Figure 4 in which the low frequency CME spectral index is about 2. This can be interpreted as being due to a large number of small-scale discontinuities in these particular CMEs.

In Figure 5 we present a comparison of the spectral indices for the slow solar wind (both IS and PS) with the CME indices. There does not appear to be any difference between the two data sets. There is no statistically significant difference between the spectral indices of CMEs and spectral indices of the solar wind confined between the high-speed streams (IS) or slow solar wind containing the heliospheric current sheet. Thus the turbulence within CMEs is more like that in the slow wind than that in wind from coronal holes.

On Magnetic Helicity Distribution inside CMEs

Observations show that the largescale magnetic field in CMEs has a helical structure. For many years a characteristic well ordered rotation of the magnetic field taking place over many hours or days has been used to identify CMEs in the interplanetary space [*Burlaga et al.*, 1981; *Lepping et al.*, 1990; *Gosling*, 1990; *Farrugia et al.*, 1992; *Bothmer and Schwenn*, 1994; *Mirubashi*, 1996]. Evidence that the rotations within magnetic clouds are indeed helical structures is found by fitting the observed data to Lundquist's model for a force-free field [*Lepping et al.*, 1990; *Mirubashi*, 1996]. Counterstreaming electrons in CMEs are considered as the evidence for a closed field topology rooted on the Sun [*Gosling et al.*, 1987]. Reconnections between the field loops associated with CMEs at the Sun can result in helical configurations of the outgoing CMEs [*Gosling*, 1990].

Because the magnetic field in CMEs is fluctuating it is interesting to study

the distribution of helical magnetic fields not only in the large scale but also in smaller scales. The invariant measure characterizing such fields is the magnetic helicity $\int \mathbf{A} \mathbf{B} dx dy dz$, where $\mathbf{A} = \text{rot}^{-1} \mathbf{B}$ is the vector potential of the magnetic field. Here we estimate the distribution of magnetic helicity inside CMEs. We adapt the approach developed in studies of interplanetary MHD turbulence [Matthaeus and Goldstein, 1982, Goldstein et al., 1995, see also references in these papers].

The basic problem in measuring the magnetic helicity in the solar wind arises due to the non-local nature of the vector potential and the fact that spacecraft data are taken at a fixed point. Simply speaking, the vector potential is not a directly observable quantity, it has to be calculated as an integral over the magnetic field in the whole volume. The non-locality problem disappears in the Fourier domain where the vector potential and the field are related locally, $B_j = i e_{jlm} k_l B_m$, (indices run from 1 to 3 corresponding to x,y,z). However the Fourier decomposition presupposes that magnetic fluctuation are periodic or homogeneous. This is the basic assumption of most turbulence studies. The time series obtained by a spacecraft at a fixed point are converted into the radial dependence of the magnetic field because the solar wind can be treated as a “frozen-in flow. Thus, at least one-dimensional Fourier spectra are available. We identify the radial direction with the x -axis.

The one-dimensional magnetic energy and magnetic helicity spectra are defined as follows

$$\langle \mathbf{B}^2 \rangle = \int E(k_x) dk_x, \quad \langle \mathbf{A} \mathbf{B} \rangle = \int H(k_x) dk_x.$$

After the use of the relation between the vector potential and magnetic field the magnetic helicity spectrum can be expressed through the correlation of the two field components transverse to the x direction

$$H(k_x) = -\frac{i}{k_x} (T_{yz}(k_x) - T_{yz}^*(k_x)),$$

where $T_{jl} = \langle B_j B_l \rangle$ is the correlation tensor in Fourier space integrated over k_y and k_z coordinates [Matthaeus and Goldstein, 1982]. For isotropic and slab type geometries of magnetic fluctuations this formula completely defines the magnetic helicity.

In this paper we do not use the one-dimensional helicity spectrum (as we did not use one-dimensional energy spectrum in the previous section), but instead we use its equivalent in the time (spatial) domain. The transformation technique is described by Goldstein *et al.*, 1994]. First, choose one of the components perpendicular to the radial direction, say $B_y(t)$, and transform it into Fourier space. Then shift the phase of each of the Fourier components by 90° . To do this multiply the real part of each Fourier component by $-i$ and the imaginary part by $+i$. Now construct a transformed data set $B_y^r(t)$ by performing an inverse Fourier transform on the “rotated” y -component. The correlation of the “rotated” and reconstructed data set $B_y^r(t)$ with the original data on the other transverse component of the field, $B_z(t)$, gives the radial distribution of magnetic helicity, RDH. In our calculations we use this measure of helicity normalized by a constant value of the mean energy of magnetic fluctuations $\langle b^2 \rangle$ in the same time interval

$$RDH = 2 \frac{\langle b_y^r(t) b_z(t) \rangle_n}{\langle b^2 \rangle} \quad (2)$$

where the subscript r indicates the 90° phase shift. The symbol $\langle \rangle_n$ indicates averaging over n points to estimate the measure on different temporal (spatial) scales. The quantities $b_y^r(t), b_z(t)$ in this formula are the fluctuating components obtained from the rotated $B_y^r(t)$ and original $B_z(t)$ by subtracting the running mean over n points. Note that our normalization using the constant value $\langle b^2 \rangle$ is different from that of Goldstein *et al.*, [1994].

Although the spectral formula for the reduced magnetic helicity discussed above has been designed and justified for homogeneous or periodic fields, Eq. (2) in itself does not limit the scales. This tempts us to apply Eq.(2) to all scales including scales only two or three times smaller than the size of CME. There is no doubt, of course, that

Eq.(2) characterizes the helical, mirror-asymmetrical properties of the magnetic field in every scale but it may not exhibit the invariant, conservative properties of the magnetic helicity.

Because of the use of Fourier transforms, data gaps will effect the results obtained using this technique. In the list of intervals used in the present analysis we found only a few cases without (or almost without) data gaps. These intervals, which include CMEs and the solar wind undisturbed by CMEs, were analyzed.

Figure 6 shows the measures of helicity calculated for the coronal hole solar wind undisturbed by CMEs. Figures 7, 8 present the measure for a magnetic cloud and a CME with bidirectional electron streaming respectively. We see that in small scales the helicity is distributed in a random fashion with alternative signs of twisting structures in both CMEs and the solar wind. In CMEs however there is a largescale helical structure which is not present in the undisturbed coronal hole wind. The helical structure for the magnetic cloud, 1978 day 302, can be interpreted as a part of the structure identified previously by fitting the data to the Lundquist solution for force-free cylindrical configuration [Lepping *et al.*, 1990]. Similar calculations for two other magnetic clouds, days 261-262, 1979 and day 038, 1981 also show largescale helical structures. Note that the reduce magnetic helicity (2) derived from the spectral approach and the helicity defined by the handiness of the force- free field [Lepping *et al.*, 1990] have opposite sign [Moffatt, 1978].

The approach used in the present paper allows the identification of helical structures in all scales not just the largest scale. The interpretation of these structures needs further work. As a preliminary step we can treat them as helical flux tubes. This gives us an opportunity to interpret different forms of “bumps” appearing in Figures 7-9. Thus, close peaks of different signs correspond to a situation when the spacecraft measurements made in the direction perpendicular to the axis of a flux tube. The measurements made strictly along the axis of a flux tube with constant values of y - and

z -components would give zero RDH. Measurements made along a direction inclined to the axis of the Lundquist-like flux tube, in which the field is radially dependent, can result in a form such as shown on the third panel of Figure 8.

We have also estimated the radial distribution of helicity for flows related to the plasma sheet and the interstream solar wind. Figure 8 gives an example of the helicity distribution in a flow associated with the plasma sheet. Although in the cases studied the magnitude of the helicity is lower than in the CMEs, there is evidence of intermediate scale helical structures in these flows. Thus all studied cases of flows coming from the closed magnetic regions of the Sun (CMEs, PS and IS) we have found large (or intermediate) scale helical structures.

Discussion

We have shown that in our data set the low-frequency spectral distribution of the magnetic energy inside CMEs is different from that in the solar wind from the coronal holes. However, we could not establish any statistically significant difference in spectral indices between turbulence in CMEs and in the interstream/plasma sheet wind. We found the difference in helical properties of the magnetic field in the solar wind from coronal holes and CMEs and the interstream/plasma sheet slow wind. We suggest that the spectral and helical differences between CMEs and coronal hole solar wind may be related to conditions in the corona where they originate. The coronal hole solar wind comes from solar regions with open magnetic configurations whereas CMEs and the solar wind associated with interstream/plasma sheet wind are related to closed magnetic configurations on the Sun. Our results indicate that turbulence on the Sun may have a different nature in the closed and open magnetic regions. For example, in closed magnetic regions the turbulence within the corona may already be well-developed Kolmogorov-like turbulence. In this model the Kolmogorov-like turbulence observed in space has been ejected from the corona directly with the CME. In the wind from coronal

holes the $1/f$ spectrum is believed to arise from the corona itself. Two models for its origin exist. In one the fluctuations in the coronal hole consist of random fluctuations (perhaps jets) and it is the sampling of this random noise by the spacecraft that produces the observed $1/f$ spectrum [Ruzmaikin *et al.*, 1995]. In the other [Matthaeus and Goldstein, 1986] the $1/f$ spectrum is due to many small reconnections in the lower corona. The association of CMEs with closed magnetic regions on the Sun also causes their largescale helical properties presumably through reconnections between the coronal magnetic loops [Gosling, 1990].

More studies are needed to firmly establish our preliminary conclusions. Work is in progress to extend the analysis by using an extensive set of the Ulysses data.

Acknowledgments. The work was performed in part for the Jet Propulsion Laboratory, California Institute of Technology, under a contract with the National Aeronautic and Space Administration.

References

- Bothmer, V., and R. Schwenn, Eruptive prominences as sources of magnetic clouds in the solar wind, *Space Sci. Rev.* **70**, 215, 1994.
- Burlaga, L. F., E. Sittler, F. Mariani, and R. Schwenn, Magnetic loop behind an interplanetary shock: Voyager, Helios, and IMP 8 observations, *J. Geophys. Res.*, **86**, 6673, 1981.
- Farrugia, C. J., L. F. Burlaga, V. A. Osherovich, and R. P. Lepping, A comparative study of dynamically expanding force-free, constant-alpha magnetic configurations with applications to magnetic clouds, in *Solar Wind Seven*, edited by E. Marsch and R. Schwenn, COSPAR, vol. 3, p. 661, Pergamon Press, New York, 1992.
- Feldman, W., Coronal structures inferred from remote sensing observations in *Robotic Exploration close to the Sun: Scientific Basis*, ed. by S. F. Habbal., AIP Conference Proc. **382**, p.9, 1996.
- Goldstein, M. L., Roberts, D. A., and C. Fitch., Properties of the fluctuating magnetic helicity in the inertial and dissipation ranges of solar wind turbulence, *J. Geophys. Res.*, , 1994
- Gosling, J. T., D. N. Baker, S. J. Bame, W.. C. Feldman, R. D. Zwickl and E. J. Smith, Bidirectional solar wind electron flux events, *J. Geophys. Res.*, **92**, 8519, 1987.
- Gosling, J. T., Coronal mass ejections and magnetic flux ropes in interplanetary space, in *Physics of Magnetic Flux Ropes*, edited by C. T. Russell and E. Priest, p. 365, AGU, 1990.
- Gosling, J. T., Physical nature of the low-speed solar wind, in *Robotic Exploration close to the Sun: Scientific Basis*, ed. by S. F. Habbal., AIP Conference Proc. **382**, p.17, 1996.
- Hirshberg, J., S. J. Bame, and D. E. Robins, Solar flares and solar wind helium enrichments: July 1965- July 1967, *Solar Phys.*, **23**, 467, 1972.
- Hundhausen, A J., Coronal mass ejections: A summary of SMM observations from 1980 and 1984-1989, in *The Many Faces of the Sun*, edited by K. Strong, J. Saba, and B. Haisch, Springer-Verlag, New York, 1996.

- Lepping, R. P., J. A. Jones, and L. F. Burlaga, Magnetic field structures of interplanetary magnetic clouds at 1 AU, *J. Geophys. Res.*, *95*, 11,957, 1990.
- Marsch, E., and C. Y. Tu, On the radial evolution of MHD turbulence in the inner heliosphere, *J. Geophys. Res.*, *95*, 8211, 1990.
- Matthaeus, W.H., and M. L. Goldstein, Measurement of the Rugged invariants of magnetohydrodynamic turbulence in the solar wind, *J. Geophys. Res.*, *87*, 6011, 1982.
- Matthaeus, W.H., and M. L. Goldstein, Low-frequency 1/f noise in the interplanetary magnetic field, *Phys. Rev. Lett.*, *57*, 485, 1986.
- Mirubashi, K., Interplanetary flux ropes and solar filaments, *J. Geophys. Res.*, to appear, 1997.
- Moffatt, K. H., *Magnetic Fields in Electrically Conducting Fluids*, Cambridge Univ. Press, Cambridge, 1978.
- Monin, A. S., and A. M. Yaglom, *Statistical Fluid Mechanics: Mechanics of Turbulence*, vol. 2, MIT Press, Cambridge, Mass., 1975.
- Neugebauer, M., and C. J. Alexander, Shuffling foot points and magnetohydrodynamic discontinuities in the solar wind, *J. Geophys. Res.*, *96*, 9409, 1991.
- Roberts, D. A., and M. L. Goldstein, Turbulence and waves in the solar wind, in *US National Report to International Union of Geodesy and Geophysics, 1987- 1990*, Suppl. to *Rev. Geophys.*, *29*, edited by M. A. Shea, p. 932, AGU, Washington, D. C., 1991.
- Ruzmaikin, A., J. Feynman, B. E. Goldstein and E. J. Smith, Intermittent turbulence in solar wind from the south polar hole, *J. Geophys. Res.*, *100*, 3395, 1995.
- Ruzmaikin, A., B. E. Goldstein, E. J. Smith, and A. Balogh, On the origin of the 1/f spectrum of fluctuations in the solar wind, in *Solar Wind Eight*, edited by D. Winterhalter, J. Gosling, S. R. Habbal, W. S. Kurth, and M. Neugebauer, AIP Conference Proc. 382, p.225, 1996.
- Tu, C. Y., and Marsch, E., MHD structures, waves and turbulence in the solar wind, Kluwer Acad. Publ., Dordrecht, 1995.

Zwickl, R. D., J. R. Asbridge, S. J. Bame, W. C. Feldman, J. T. Gosling, and E. J. Smith,
Plasma properties of driver gas following interplanetary shocks observed by ISEE- 3, in
Solar Wind Five; edited by M. Neugebauer, NASA Conf. Proc., CP-2280, p.711, 1983.

A. A. Ruzmaikin, J. Feynman, and E. J. Smith Jet Propulsion Laboratory, California
Institute of Technology, 4800 Oak Grove Drive, Pasadena, CA 91109. (e-mail: aruz-
maikin@jplsp.jpl.nasa.gov; jfeynman@jplsp.jpl.nasa.gov; esmith@jplsp.jpl.nasa.gov)

Received January, 1997

Table 1. Fast and Slow Wind Intervals Used in Our Analysis of ISEE 3 Data and Spectral Indices Found

Year Day/UT	Identification	Speed, km/s	SpIndex in HFR	SpIndex in LFR
1978 270/1720 - 271/2020	CH	626	$1.58 \pm .05$	$1.20 \pm .03$
1978 353/1050 - 355/0945	CH	629	$1.53 \pm .04$	$1.24 \pm .02$
1979 038/1006 - 041/1500	CH	350	$1.60 \pm .04$	$1.15 \pm .03$
1979 131/0940 - 133/1010	CH	504	$1.58 \pm .03$	$1.02 \pm .01$
1979 166/2020 - 168/0400	CH	436	$1.57 \pm .02$	$1.33 \pm .02$
1978 234/0500 - 239/0000	IS	331	$1.78 \pm .03$	$1.26 \pm .04$
1978 258/0700 - 259/1900	IS	331	$1.72 \pm .02$	$1.53 \pm .02$
1978 262/0730 - 263/0100	IS	298	$1.76 \pm .03$	$1.79 \pm .04$
1978 308/2100 - 310/1825	IS	329	$1.67 \pm .04$	$1.39 \pm .02$
1978 360/0000 - 362/0140	IS	397	$1.86 \pm .03$	$1.32 \pm .02$
1978 236/0200 - 237/0900	PS	311	$1.82 \pm .02$	$1.34 \pm .01$
1978 255/0700 - 255/2130	PS	365	$1.89 \pm .02$	$1.46 \pm .01$
1978 263/1305 - 264/0200	PS	289	$1.98 \pm .03$	$1.57 \pm .03$
1978 290/0300 - 290/1700	PS	364	$1.78 \pm .02$	$1.30 \pm .05$
1978 310/1825 - 311/1500	PS	301	$1.78 \pm .03$	$1.49 \pm .03$

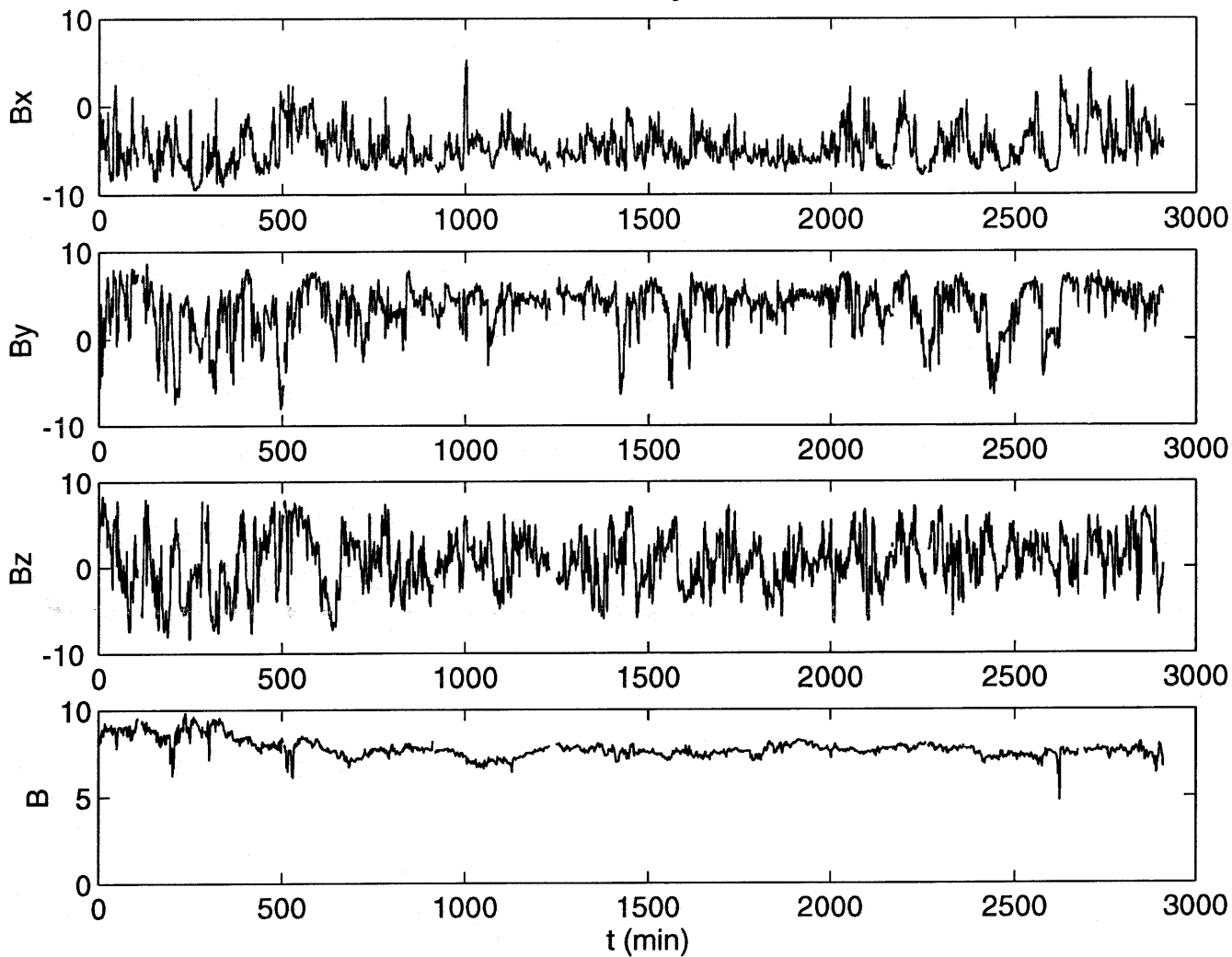
The identification marks stand for: CH = solar wind from coronal holes, IS = interstream solar wind, PS = flows surrounding sector boundaries (“plasma sheets”), SpIndex in HFR = Spectral Index in High-Frequency Region, SpIndex in LFR = Spectral Index in Low-Frequency Region

Table 2. CMEs Used in Our Analysis of ISEE 3 Data and Spectral Indices Found

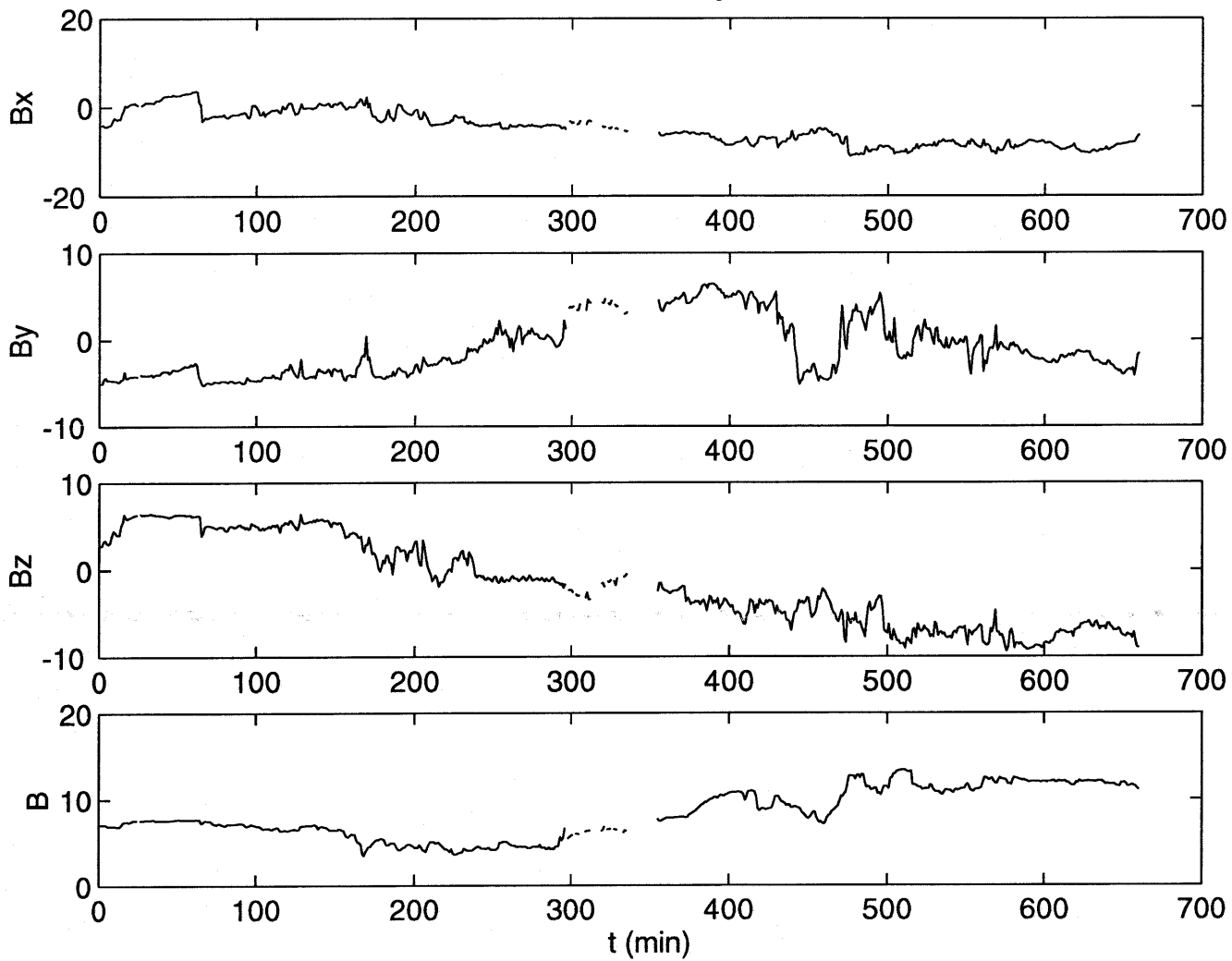
Year Day/UT	Identification	Speed, km/s	SpIndex in HFR	SpIndex in LFR
1978 253/0200 - 253/1800	BES	440	$1.73 \pm .05$	$1.59 \pm .04$
1978 272/1150 - 272/2350	BES	701	$1.74 \pm .02$	$2.30 \pm .01$
1978 345/0030 - 346/0200	BES	282	$1.66 \pm .03$	$1.66 \pm .03$
1978 357/0100 - 357/1230	BES	503	$1.82 \pm .04$	$1.79 \pm .02$
1979 007/0400 - 007/1500	BES	544	$1.73 \pm .02$	$1.72 \pm .10$
1979 008/0615 - 008/2400	BES	432	$1.78 \pm .02$	$1.58 \pm .09$
1979 093/1930 - 095/0115	BES	448	$1.84 \pm .05$	$1.60 \pm .05$
1979 095/0950 - 096/0500	BES	698	$1.75 \pm .02$	$2.33 \pm .03$
1979 115/1110 - 115/2330	BES	620	$1.72 \pm .03$	$1.44 \pm .03$
1979 149/2100 - 151/0800	BES	485	$1.64 \pm .07$	$1.51 \pm .02$
1979 277/1005 - 278/0550	BES	351	$1.87 \pm .02$	$1.48 \pm .04$
1979 337/0630 - 337/1800	BES	372	$1.75 \pm .03$	$1.85 \pm .05$
1978 239/1900 - 240/1600	MC	460	$1.66 \pm .05$	$1.64 \pm .06$
1978 302/2300 - 304/0000	MC	392	$1.74 \pm .03$	$2.14 \pm .04$
1979 261/1500 - 262/1800	MC	367	$1.75 \pm .01$	$1.43 \pm .05$
1981 038/0700 - 039/1200	MC	446	$1.50 \pm .03$	$1.34 \pm .05$
1982 268/1700 - 269/1500	MC	482	$1.70 \pm .02$	$1.87 \pm .03$
1982 327/2100 - 328/1200	MC	547	$1.95 \pm .04$	$1.46 \pm .09$

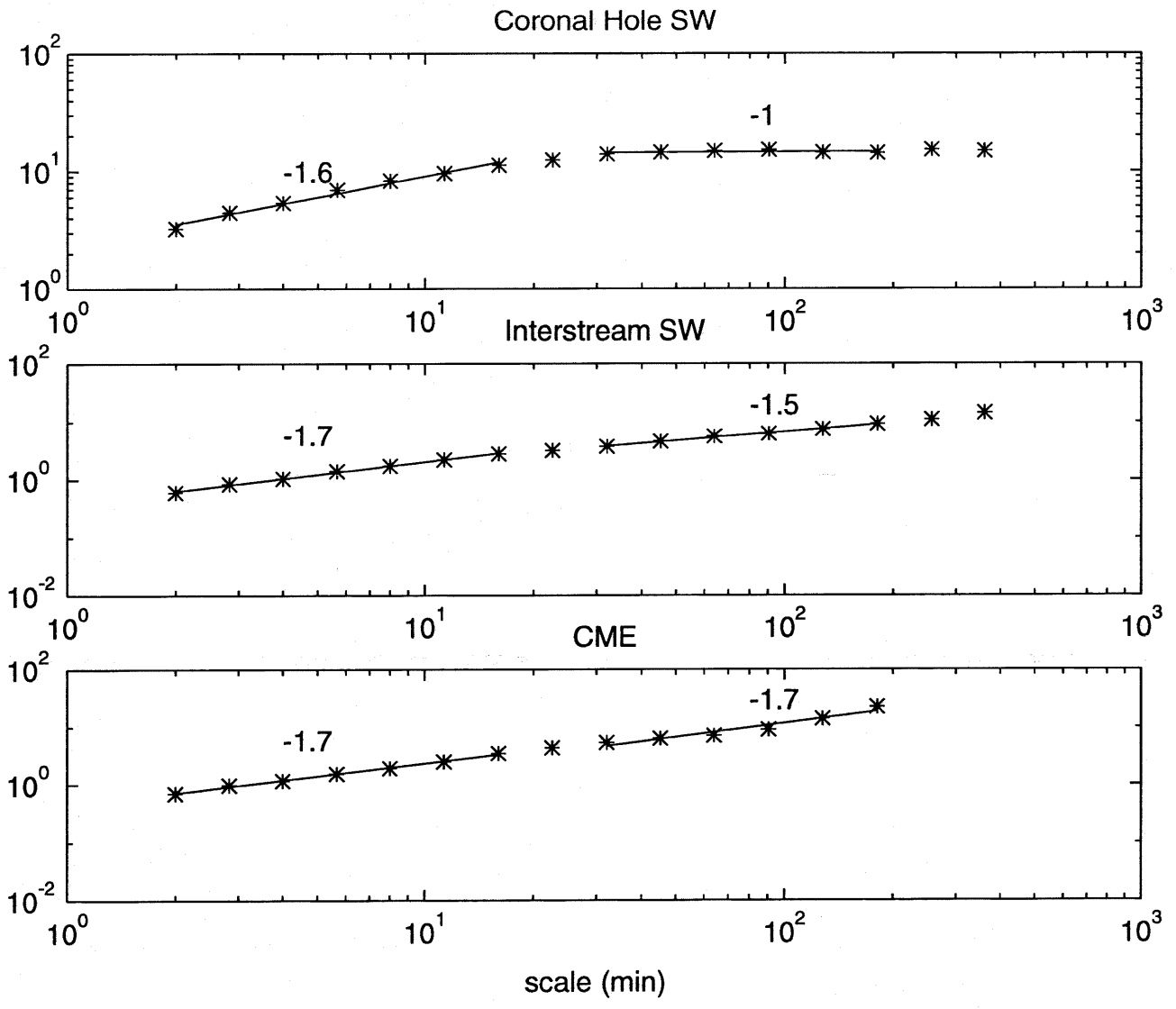
The identification marks stand for: BES = bidirectional electron streaming, MC = magnetic cloud, SpIndex in HFR = Spectral Index in High-Frequency Region, SpIndex in LFR = Spectral Index in Low-Frequency Region

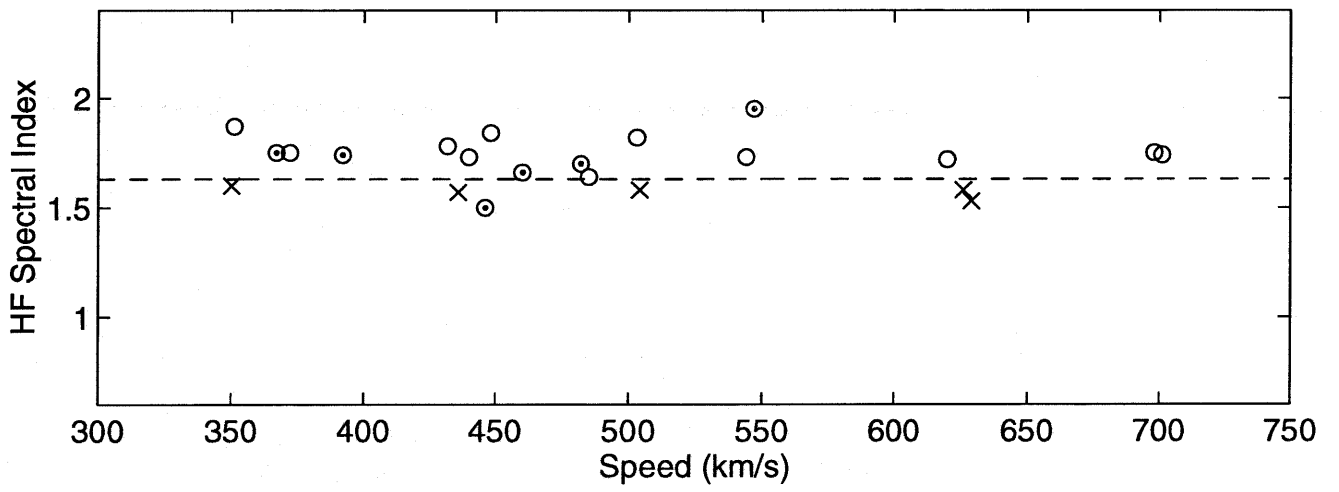
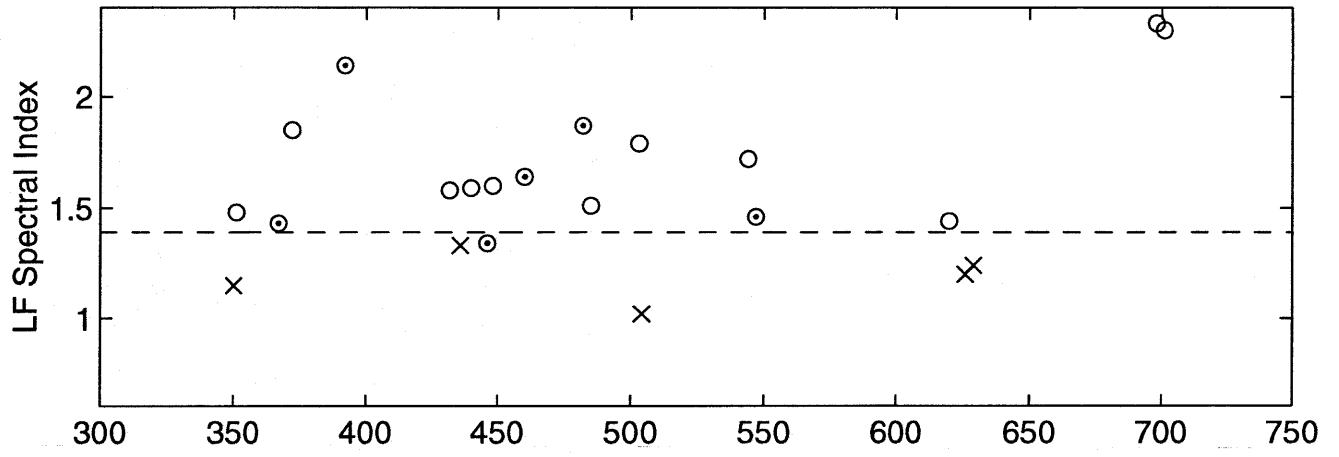
ISEE 3 1979 days 131-133

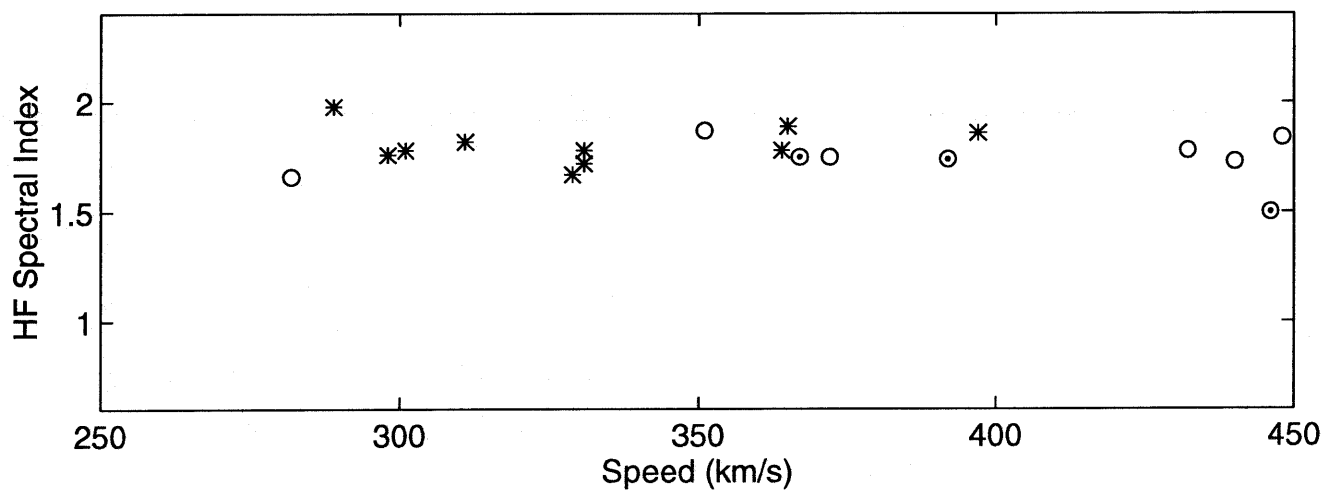
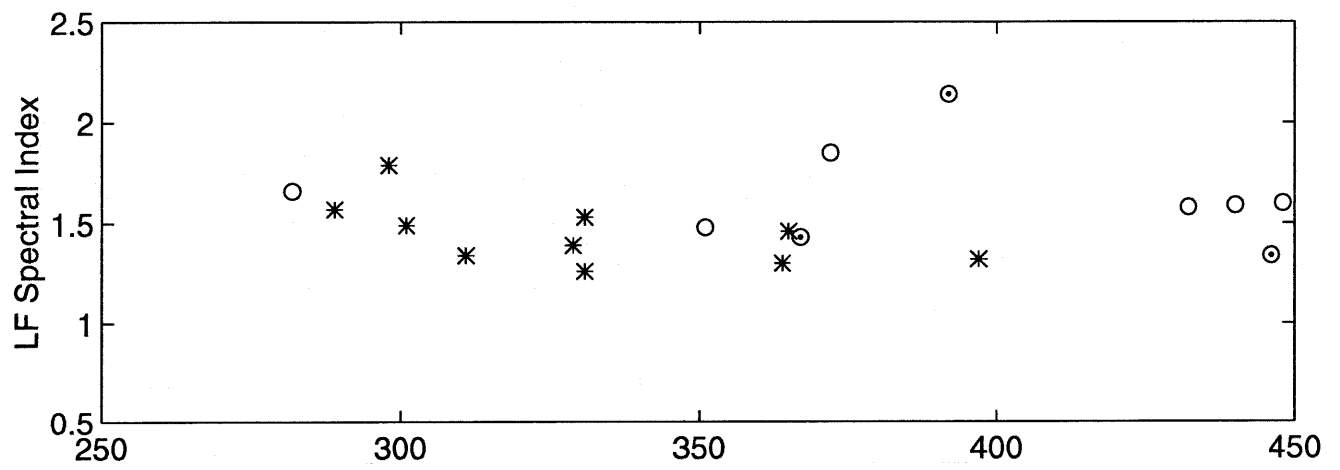


ISEE 3 1979 day 007

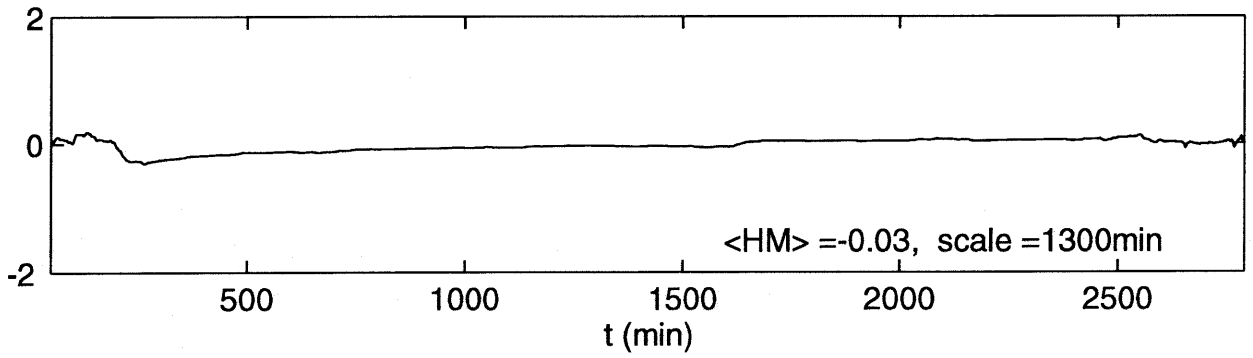
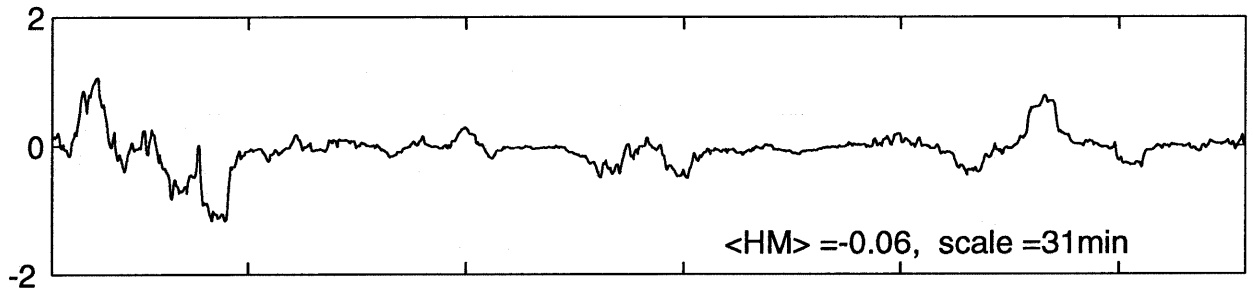
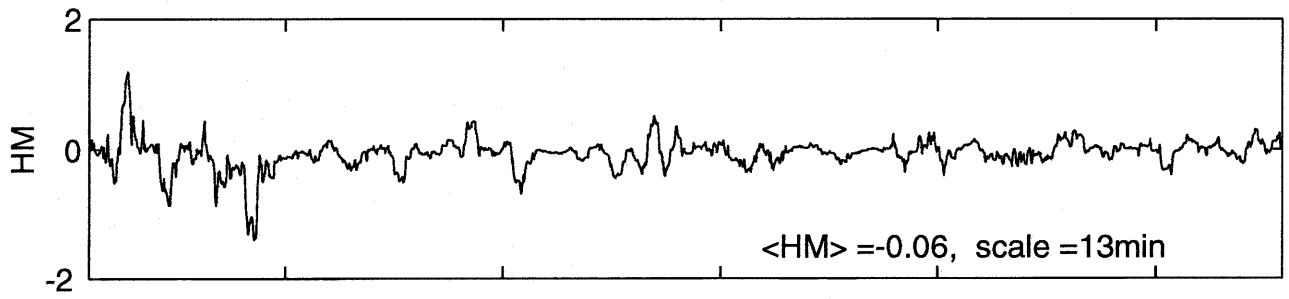




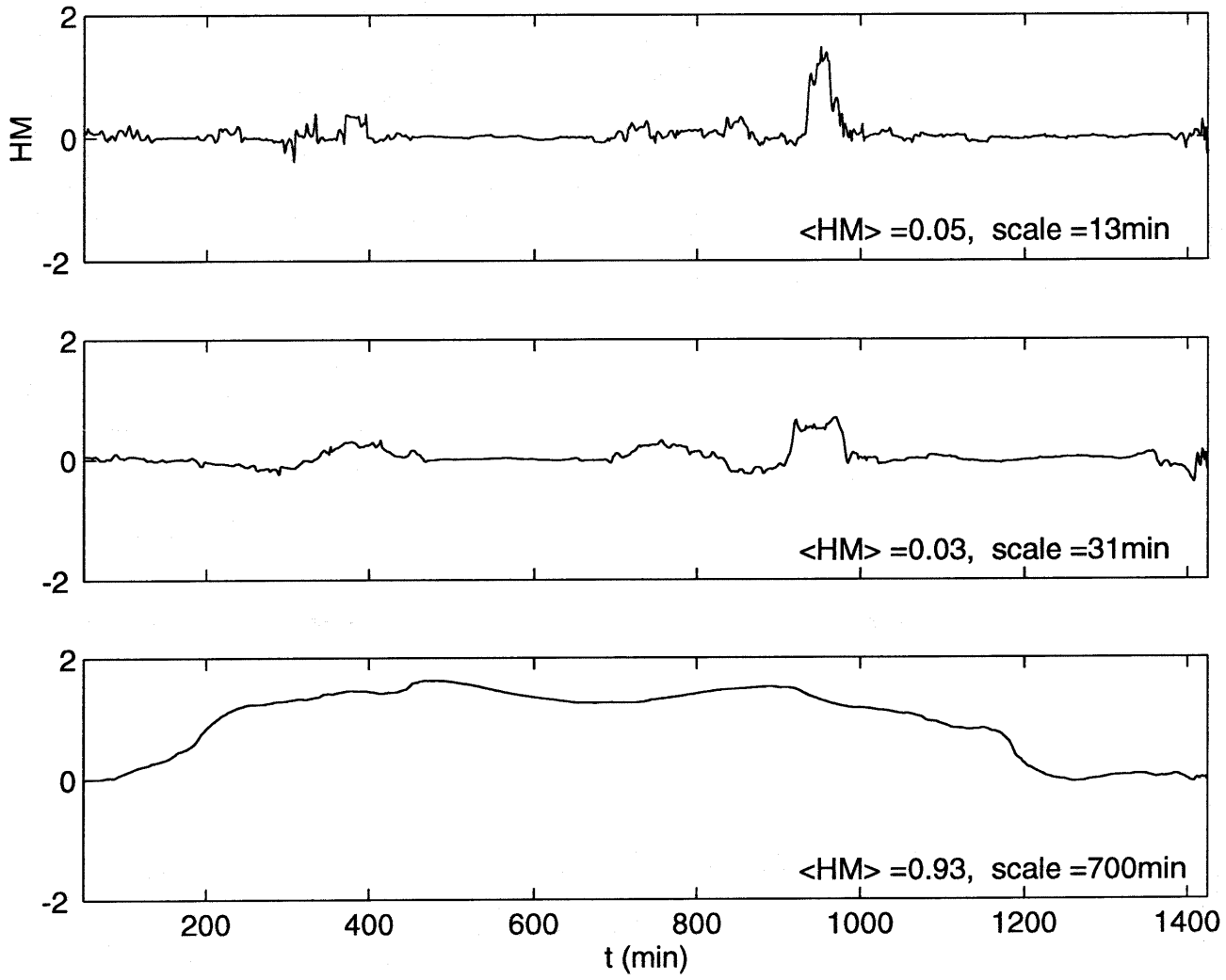




ISEE 3 1979 days 131-133



ISEE 3 1978 day 302



ISEE 3 1978 days 263-264

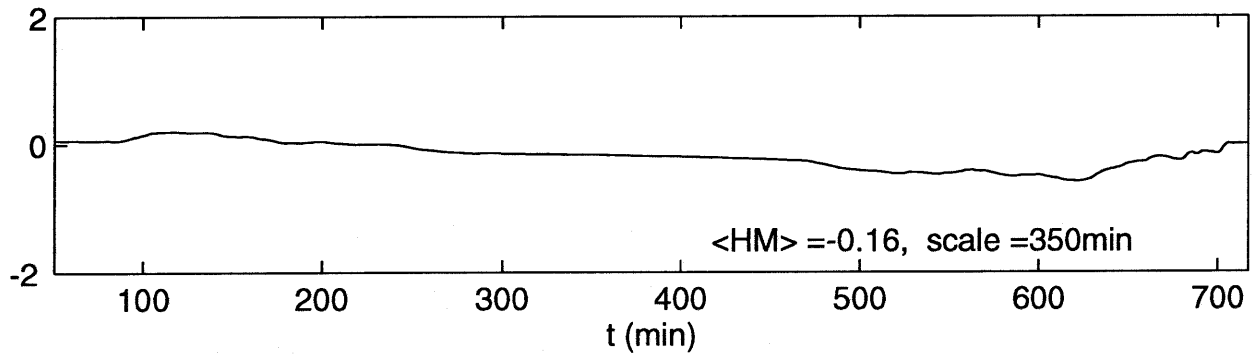
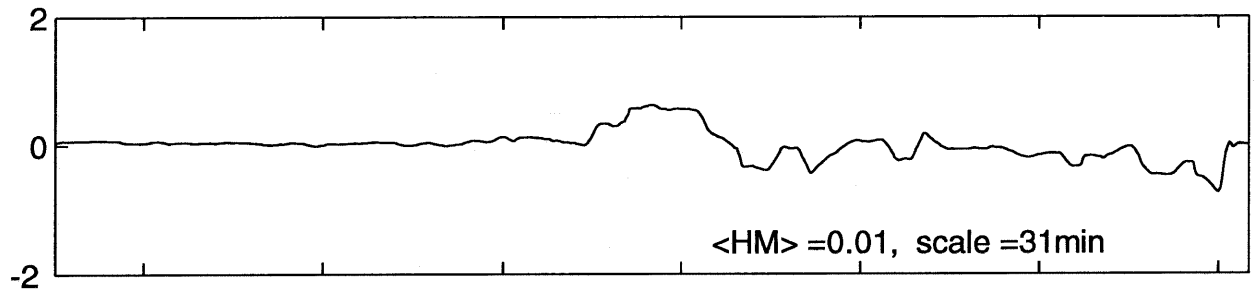
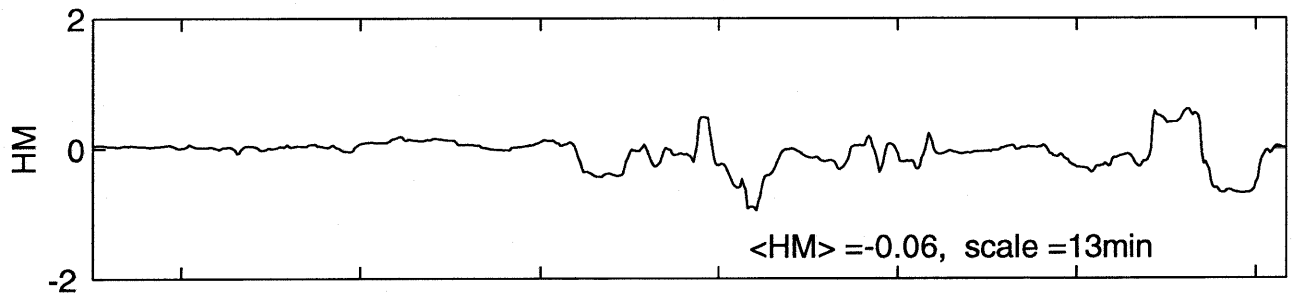


Figure Captions

Figure 1. The 1 min. averaged components and magnitude of the magnetic field in the solar wind coming from a coronal hole (1979 days 131-133). In the co-ordinate system used throughout this paper the axis x is along the radial direction and positive outward from the Sun, y is in the ecliptic plane and positive in the direction of planetary motion and z is perpendicular to x and y and positive north.

Figure 2. The 1 min. averaged components and magnitude of the magnetic field in a CME defined by bidirectional electron streaming (1979 day 007).

Figure 3. Examples of structure functions of the magnetic field. The top panel is the structure function for the solar wind from a coronal hole (see Figure 1). The speed of this flow is 504 km/s. The middle panel is the structure function for a slow interstream wind (331 km/s). The lower panel is the structure function for a CME (see Figure 2) moving with the speed of 544 km/s. The rounded spectral indices are given above the fitted lines.

Figure 4. Spectral indices versus flow speed for solar wind from coronal holes (x) and CMEs. Indices for CMEs defined by bidirectional streaming are given by (o). Those for CMEs defined by magnetic clouds are marked with a point inside the symbol "o". Indices for CMEs tend to be a little larger, especially at low frequencies. There is no speed dependence.

Figure 5. Spectral indices versus speed for slow wind (IS and PS) flows (*) and CMEs. There is no dependence on either speed or type of solar wind.

Figure 6. The measure of magnetic helicity at three scales for the solar wind from the coronal holes. Data are taken from Figure 1. Notice the absence of largescale helical structures at the largest 1300 min scale used. For comparison with the CME's cases note that there is also no structures at 700 min.

Figure 7. The measure of magnetic helicity at three scales for the magnetic cloud 1978 day 302. A largescale helical structure is present. Note there few if any structures at the intermediate scales not shown in this Figure

Figure 8. The measure of magnetic helicity at three scales for the plasma sheet flow, 1977 day 263.